

EPJ E

Soft Matter and
Biological Physics

EPJ.org
your physics journal

Eur. Phys. J. E (2019) **42**: 18

DOI 10.1140/epje/i2019-11785-y

Breakup of finite-size liquid filaments: Transition from no-breakup to breakup including substrate effects

A. Dziejic, M. Nakrani, B. Ezra, M. Syed, S. Popinet
and S. Afkhami

edp sciences



 Springer

Breakup of finite-size liquid filaments: Transition from no-breakup to breakup including substrate effects^{*}

A. Dzedzic¹, M. Nakrani¹, B. Ezra¹, M. Syed¹, S. Popinet², and S. Afkhami^{1,a}

¹ Department of Mathematical Sciences, New Jersey Institute of Technology, Newark, NJ 07102, USA

² Sorbonne Université, Centre National de la Recherche Scientifique, Institut Jean le Rond d'Alembert, F-75005, Paris, France

Received 3 May 2018 and Received in final form 2 August 2018

Published online: 20 February 2019

© EDP Sciences / Società Italiana di Fisica / Springer-Verlag GmbH Germany, part of Springer Nature, 2019

Abstract. This work studies the breakup of finite-size liquid filaments, when also including substrate effects, using direct numerical simulations. The study focuses on the effects of three parameters: Ohnesorge number, the ratio of the viscous forces to inertial and surface tension forces, the liquid filament aspect ratio, and where there is a substrate, a measure of the fluid slip on the substrate, *i.e.* slip length. Through these parameters, it is determined whether a liquid filament breaks up during the evolution toward its final equilibrium state. Three scenarios are identified: a collapse into a single droplet, the breakup into one or multiple droplets, and recoalescence into a single droplet after the breakup (or even possibly another breakup after recoalescence). The results are compared with the ones available in the literature for free-standing liquid filaments. The findings show that the presence of the substrate promotes the breakup of the filament. The effect of the degree of slip on the breakup is also discussed. The parameter domain regions are comprehensively explored when including the slip effects. An experimental case is also carried out to illustrate the collapse and breakup of a finite-size silicon oil filament supported on a substrate, showcasing a critical length of the breakup in a physical configuration. Finally, direct numerical simulations reveal striking new details into the breakup pattern for low Ohnesorge numbers, where the dynamics are fast and the experimental imaging is not available; our results therefore significantly extend the range of Ohnesorge number over which filament breakup has been considered.

1 Introduction

The breakup of liquid jets has been a subject of extensive research [1–5], with applications, for instance, ranging from droplet generation in microfluidics, paint spraying, and ink-jet printers, to biological and geological systems. Theoretical, computational and experimental studies of the breakup of finite-size free-standing filaments (of Newtonian liquids) exist in the literature; see *e.g.* [1, 5–8]. Studies of the breakup of finite-size liquid filaments involving substrate effects, however, have so far been very limited; see *e.g.* [9–11]. This is mainly due to difficulties associated with the presence of a substrate. The study in [10] reports on simulations of liquid filaments breaking up into droplets on partially wetting substrates, however ignoring the inertial effects. The study in [11] reports on the retraction of liquid filaments on substrates under par-

tially wetting conditions, the study however is limited to the evolution just before the breakup. Finally, the work in [9] reports on experimental and numerical studies on the breakup of finite-size, nano- and microscale, liquid metal filaments on a substrate. The work however is limited to a small range of parameter space. Our work here differs from previous studies in that we explore the parameter domain regions comprehensively, including the substrate slip effects, by solving the full three-dimensional Navier-Stokes equations based on a Volume-of-Fluid interface tracking method that can accurately and efficiently (adaptively) model the breakup and coalescence of fluid interfaces [12].

The experimental work of Pita *et al.* [7] is the main motivation of the computational study carried out in this paper. In [7], the authors experimentally show that a finite-size liquid filament can collapse into one droplet or break up to multiple droplets, depending on the viscosity and the initial dimensions of the filament. This phenomenon can be explained as the competition between surface tension, that drives either the pinching-off or shortening of the filament, and viscous forces, resisting the deformation [1]. In the work of Pita *et al.* [7] and Notz and Basaran [5], two

^{*} Contribution to the Topical Issue “Flowing Matter, Problems and Applications”, edited by Federico Toschi, Ignacio Pagonabarraga Mora, Nuno Araujo, Marcello Sega.

^a e-mail: shahriar.afkhami@njit.edu

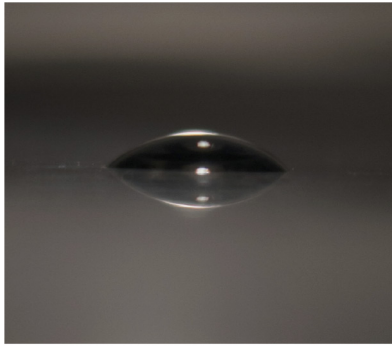


Fig. 1. The contact angle is measured from photographic images of droplets formed on the substrate using MATLAB® image processing toolbox. The measured contact angle is about 30° . Photographs are taken after the filament has broken up into droplets and the resulting droplets reached an equilibrium state.

dimensionless quantities are identified as the relevant parameters controlling the final outcome: the filament aspect ratio and the Ohnesorge number. The Ohnesorge number, denoted by Oh , represents the significance of surface tension and viscosity ($Oh = \frac{\mu}{\sqrt{\rho\sigma R_0}}$) where the liquid viscosity, density, and surface tension are denoted by μ , ρ , and σ , respectively, and R_0 is the filament initial radius. The aspect ratio, $AR = \frac{L_0}{R_0}$, represents the ratio between the half of the initial length, denoted by L_0 here, and the initial radius of the filament, R_0 .

The experimental study in [7] explores the breakup of finite-size free-standing liquid filaments over the range $0.003 < Oh < 10$, for filaments with $1 < AR < 70$. The results in [7] show, in agreement with the prior computational investigation in [5], that within the range of considered Oh and AR , the filament does not break up for $AR < 6$, regardless of the Oh number, and that no filament breakup occurs for $Oh > 1$, regardless of AR values. The work in [7] also identifies the critical filament aspect ratios, above which the filament breaks up, for a range of $0.003 < Oh < 10$.

In this paper, we carry out an investigation of the collapse and breakup of finite, millimeter size, liquid filaments on a substrate. We first motivate our study by conducting experiments to show the unstable evolution of liquid filaments deposited on a substrate that leads to either the collapse to a single droplet or the breakup. We show this transition by increasing the length of the filament deposited on a substrate, illustrating the existence of a threshold, above which the filament breaks up into multiple droplets. A similar study has been carried out previously in the context of pulsed laser-induced dewetting of nanometer size geometries [9].

The experiments are conducted using 28000 molecular weight polydimethylsiloxane deposited on a plastic substrate coated with Rust-Oleum® NeverWet® treatment to make the substrate partially wetting. We ensured the wetting reproducibility by the treatment process through measuring the contact angle by taking photographic images of the resulting droplets on the substrate (see fig. 1),

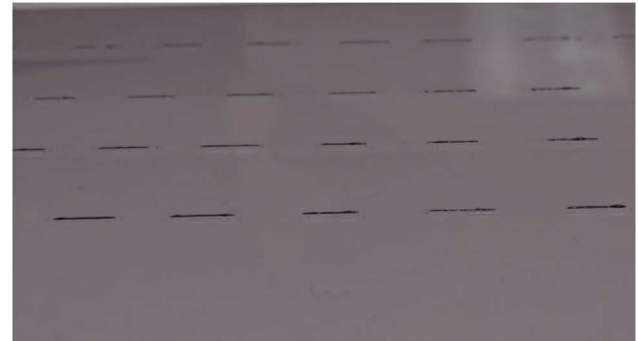
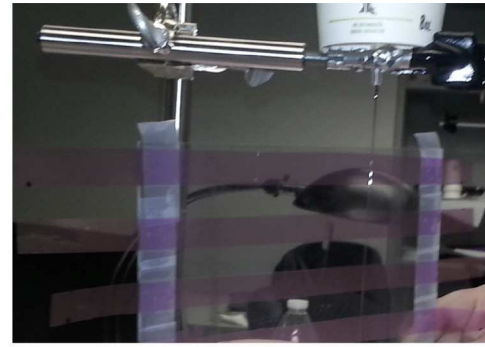


Fig. 2. Illustration of the experimental setup: filaments are captured by swiping the substrate through the liquid stream flowing out of the nozzle attached to a container filled with polydimethylsiloxane up to a certain height (top). Cellophane (pink) strips are taped to the plate to produce filaments of various lengths. The substrate is then immediately placed on a horizontal surface and cellophane strips are removed (bottom). The initial width of the filaments is about 1 mm.

using MATLAB® image processing toolbox. We adopt an experimental procedure similar to the one reported in [13], where filaments are captured from a jet flowing out of a nozzle attached to a container filled with polydimethylsiloxane up to a certain height. In order to produce filaments of various lengths, we tape the substrate with cellophane strips (see fig. 2). The substrate is then swiped through the liquid stream to create an even, straight line. The substrate is then immediately placed on a horizontal surface, after which the cellophane strips are removed (see fig. 2). The filaments are then left undisturbed to retract to form droplets (see fig. 3). This process is repeated to ensure the reproducibility of the results, as well as the controllability of the length. We carry out the above procedure for $9 \text{ mm} \leq 2L_0 \leq 17 \text{ mm}$ and show the results in fig. 3. As shown, there is a critical length below which the filament does not break up but rather collapses to a single droplet. The transition from collapse to breakup can be described as a competition between the capillary driven end retraction, the Rayleigh-Plateau-type instability mechanism [14], and the viscous dissipation due to the presence of the substrate [10,9]. Assuming typical physical properties of the polydimethylsiloxane at room temperature, *e.g.* $\mu = 1 \text{ Pa}\cdot\text{s}$, $\rho = 971 \text{ kg/m}^3$, $\sigma = 0.02 \text{ N/m}$, we estimate $Oh \approx 17$, where we calculate $R_0 \approx 0.17 \text{ mm}$ based on the initial filament thickness of approximately 1 mm and the contact angle of 30° (*i.e.*, R_0 is the radius

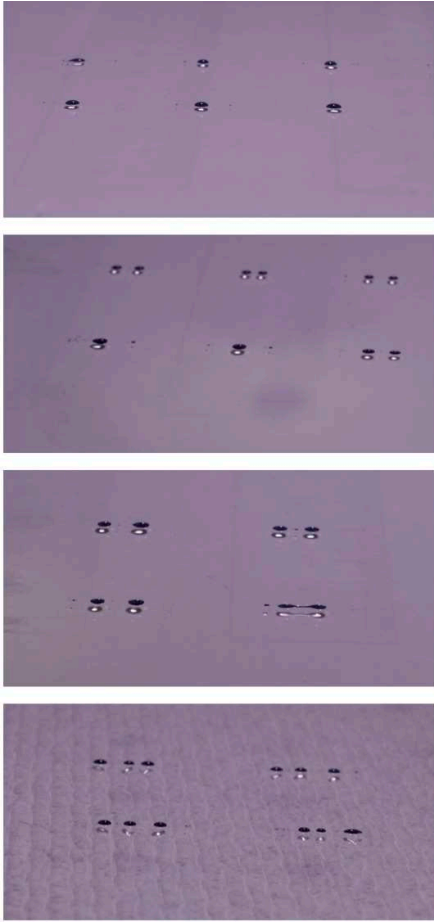


Fig. 3. Photographic images of the polydimethylsiloxane filaments increasing in length, $2L_0 \approx 9$ mm, 11 mm, 15 mm and 17 mm from top to bottom. The initial width of the filaments is about 1 mm. While the filament of length 9 mm collapses into single drops, filaments of length 11 mm and above break up into multiple droplets. $Oh \approx 17$ and $R_0 \approx 0.17$ mm.

of a cylinder whose cross sectional area is equivalent to that of the filament resting on the substrate with a given width and contact angle). This result is interesting because the experimental evidence in [7] suggests that no filament breakup can be observed for $Oh > 1$, regardless of the filament initial aspect ratio. Our experiments however show that the presence of the substrate can promote breakup leading to a much larger Oh for which the breakup can occur.

In what follows, we will focus on the effect of the interaction with the substrate on the filament breakup. We explore the boundary between breakup and no-breakup regimes as a function of Oh and AR for various substrates characterized by different slip lengths. We report the results of numerical simulations, extending the range of Oh that has been so far considered in the literature, as well as revealing peculiar breakup patterns for low Oh . For our study, we carry out direct numerical computations of the full Navier-Stokes equations, using Gerris code [12]. We explore the range of $2 \leq AR \leq 60$ and $10^{-3} \leq Oh \leq 14$, focusing on the effect of the degree of slip on the results.

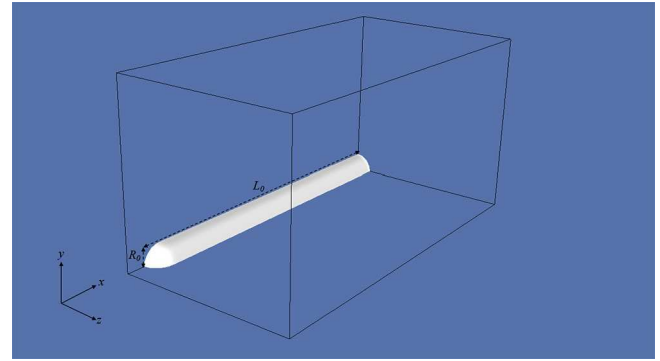


Fig. 4. Computational geometry, where R_0 is the radius and L_0 is the half length of the filament with spherical end caps. For a freely standing filament, we use a symmetry boundary condition on all computational boundaries. For a filament on the substrate, we use a symmetry boundary condition on all computational boundaries except on the bottom boundaries where the substrate is modeled.

Our study here mainly focuses on generating a large numerical dataset, by carrying out an exhaustive and systematic investigation. Additionally, our study enhances the current numerical results regarding the freely standing finite-size filaments. We hope that this work will provide a basis for future theoretical analysis, when including the substrate effects.

2 Computational setup

We numerically investigate the dependence of the breakup of a filament, either freely standing or being deposited on a substrate. Initially, a liquid filament of radius R_0 and length $2L_0$ is considered. We take advantage of the symmetries that exist in the problem and model only 1/8 of the freely standing filament or 1/4 of the filament on the substrate; see fig. 4.

For a freely standing filament, we use a symmetry boundary condition for all variables on all computational boundaries. The code for the computational setup is derived from the ‘‘Savart-Plateau-Rayleigh’’ example, which is one of the examples from the Gerris open source site [15]. When there is a substrate, we use a symmetry boundary condition on all computational boundaries except on the bottom boundaries where the substrate is modeled as either a no-slip boundary or if partial slip is allowed, we then impose the Navier slip boundary condition [16] at the substrate ($y = 0$)

$$(u, w)|_{y=0} = \lambda \partial(u, w)/\partial y|_{y=0}, \quad (1)$$

where λ is the slip length and (u, w) are the components of the velocity field tangential to the solid boundary. For issues regarding the regularization of the viscous stress singularity at the contact line, the reader is referred to [17]. When the filament is placed on a solid surface, we impose a contact angle of 90° ; this is due to the limitation of the code for having an arbitrary contact angle and the simplicity in imposing a 90° contact angle. For the details

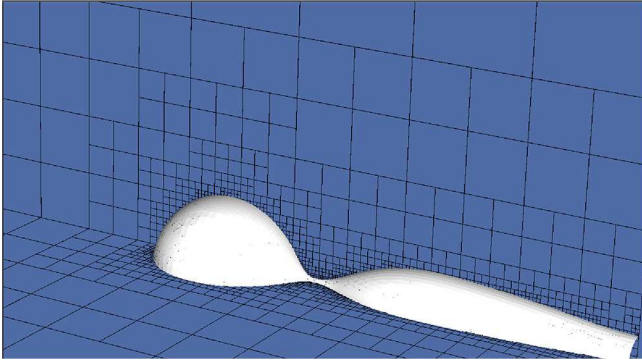


Fig. 5. Details of the adaptive mesh refinement where the resolution is adjusted so that the size of any cell containing the interface is $\Delta = 1/2^8$.

of the numerical methodologies, including the Volume-of-Fluid method for tracking the interface and for the computation of the surface tension force, the interested reader is referred to [18–20]. A computational domain of $[0, 2] \times [0, 1] \times [0, 1]$ is considered. We vary R_0 and L_0 in order to have $2 \leq \text{AR} \leq 60$. We set the surface tension $\sigma = 1$ and the filament liquid density $\rho = 1$, and vary the filament liquid viscosity according to $\mu = \sqrt{R_0 \text{Oh}}$. We set the density and viscosity ratio to approximately 800 and 50, respectively (corresponding for example to air/water physical parameters). Simulations are then performed for various Oh numbers ($10^{-3} \leq \text{Oh} \leq 14$) and slip length values ($0 \leq \lambda \leq 1$). We use dynamic adaptive mesh refinement as in [19], particularly around the breakup point, see fig. 5, and the maximum level of refinement is arbitrarily set to 8, unless stated otherwise; using an octree mesh (in 3D), the root cell is at level zero and each successive generation increases the cell level by one, *i.e.* the smallest mesh size $\Delta = 1/2^8$. We note that for the substrate-supported filaments, Oh number is also defined using R_0 . This is because the presence of a substrate only slightly modifies the Rayleigh-Plateau analysis, see *e.g.* [21, 9], and therefore the relevant length scale should not change.

We define the transition between breakup and no-breakup as whether the filament breaks up at anytime during its evolution toward a final equilibrium state. During the evolution, two main scenarios can be identified: i) no breakup and collapse into a single droplet, see fig. 6(a), or ii) the breakup of the filament, see fig. 6(b). We have checked and made sure this characterization is independent of the mesh resolution; see fig. 6(c) that shows the breakup scenario for a higher resolution compared to the case shown in fig. 6(b). Although the results show quantitative differences, whether the breakup occurs or not is independent of the grid size—we have also checked this for other simulations. Interestingly, for free-standing jets, at the transition AR, the broken up filament always condenses into a single droplet, regardless of the Oh number, see for example, fig. 6(b). This is quite different from the filaments that are supported by a substrate; we will show later that in that case, the final configuration can also

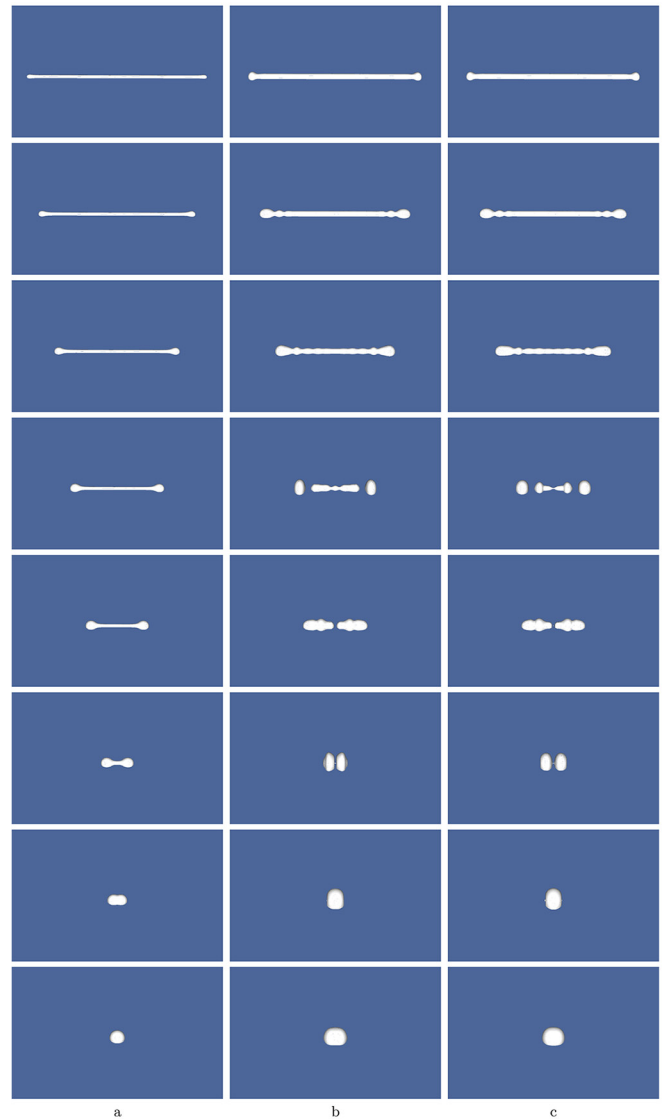


Fig. 6. Simulations for free-standing jets: (a) $(\text{Oh}, \text{AR}) = (0.8, 49)$ and (b), (c) $(\text{Oh}, \text{AR}) = (0.015, 28)$ for (8, 9) levels of refinement. Only the top half of the filament is shown.

be two (or multiple) distinguished droplets (without re-coalescence). For scenario ii) above, we can also identify a number of cases: ii-a) the filament breaks up into two droplets that eventually re-coalesce into one single drop, see fig. 7(a); ii-b) the filament breaks up into two droplets, then condenses into a single drop that breaks up again due to significant inertia, and eventually re-coalesces into a single droplet because of strong oscillations, see fig. 7(b); and ii-c) the same as case ii-b) but without the final re-coalescence, so two distinct drops form at the end, see fig. 7(c).

3 Results and discussions

We first validate our numerical results by comparing them against the experimental observations in [7] for standing liquid jets. We carry out full 3D simulations despite the

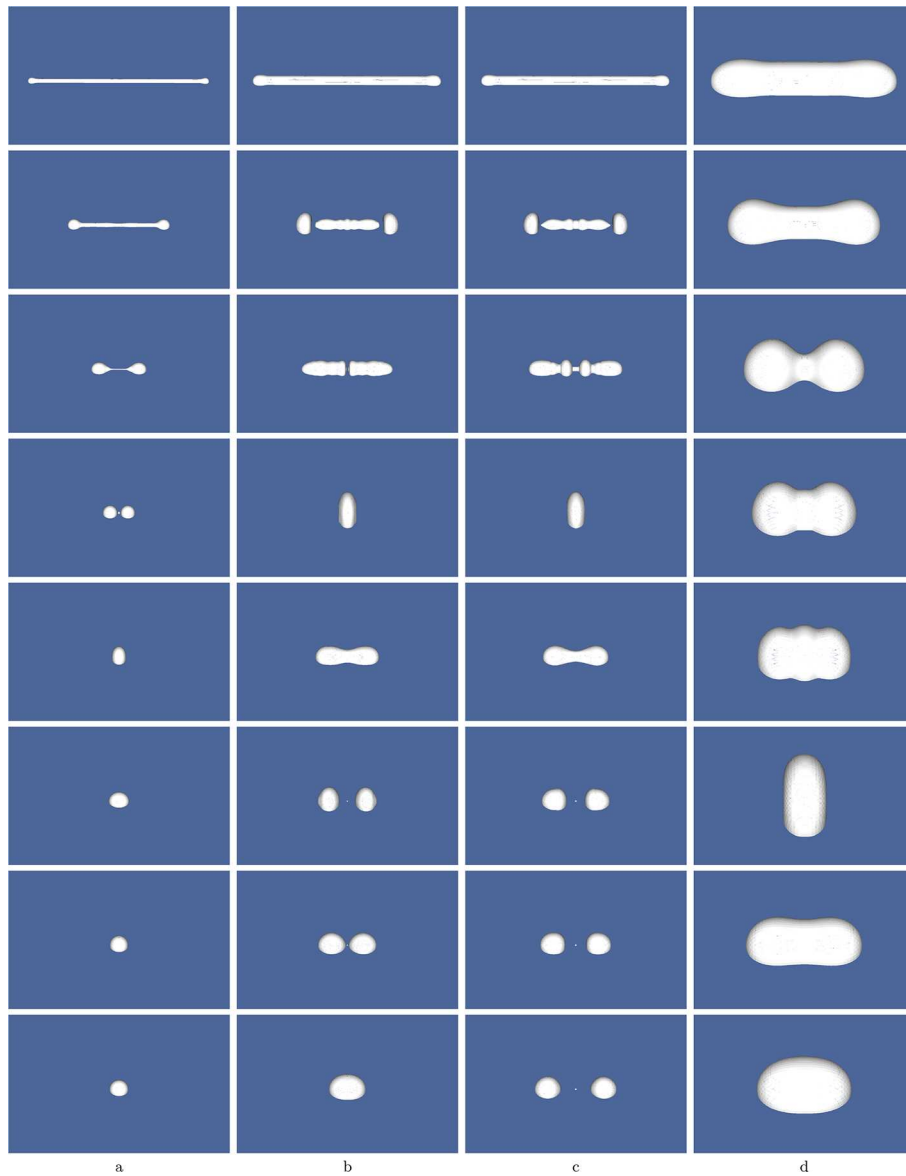


Fig. 7. Simulations for free-standing jets: (a) $(Oh, AR) = (0.4, 49)$, (b) $(Oh, AR) = (0.00125, 18)$, (c) $(Oh, AR) = (0.001, 18)$, and (d) $(Oh, AR) = (0.015, 5)$. Only the top half of the filament is shown.

fact that due to axial symmetry in this case, axisymmetric simulations suffice. However, apart from the consistency with the results of the substrate-supported filaments, for visualization purposes, we also perform 3D computations for free-standing filaments. As discussed in [8], for viscous liquid filaments, the transition from collapse to breakup can be described as a competition between the capillary driven end retraction and the Rayleigh-Plateau-type [14] instability mechanism. Filaments with a small aspect ratio do not break up irrespective of the Oh number; in this case, end pinching does not have time to develop and the whole filament collapses into a single drop; see *e.g.* fig. 7(d). Very viscous filaments ($Oh > 1$) are also always stable regardless of AR; in this case, the Rayleigh-Plateau mechanism is not operative to cause the filament to break up; see *e.g.* fig. 6(a). The breakup occurs when the breakup

time due to Rayleigh-Plateau instability is comparable to the time required for the end pinching to happen; see *e.g.* fig. 7(a).

Figure 8 presents the comparison of our numerical results with the experimental data in [7]. As shown, there is a clear agreement between our results and the experimental ones. The breakup transition predicted numerically is also shown to agree with the observations in [7]. Additionally, we extend the parameter space to smaller values of Oh ($O(0.001)$), where prior results are not available in the literature for that range. In this range, the dynamics is very fast and surface capillary waves do not have enough time to grow. However, it appears from the numerical results that the boundary between the breakup and no-breakup remains unchanged when decreasing Oh below about 0.01. This is the region which was not explored in the

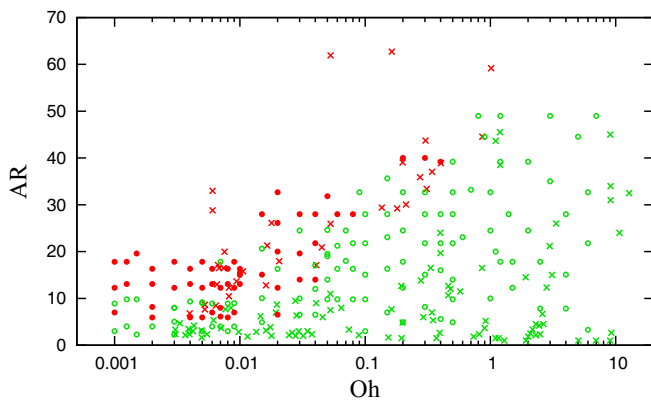


Fig. 8. Breakup and no-breakup results plotted as a function of Oh versus AR: breakup (●) and no-breakup (○). Experimental results in [7]: breakup (×) and no-breakup (×).

experiments in [7], suggesting that there is an AR of about 10, above which the breakup always occurs for $Oh < 0.01$.

Interestingly, the simulations reveal a non-continuous behavior in the breakup and no-breakup regime when AR is varied for a fixed Oh number and when the Oh number is sufficiently small. For example, consider $Oh = 0.02$, where the simulations show breakup for $AR = 12$, no-breakup for $AR = 16$, and breakup for $AR = 26$; see fig. 9. (We note that this behavior is not presented in the experimental data in [7], mainly because in the region that the numerical results show non-continuity in breakup to no-breakup, there are either limited or no experimental observations; this can be due to the fact that the breakup occurs on a very fast time scale and therefore high framing speeds are needed to capture fast breakups—the numerical simulations can indeed be very useful here. As authors in [7] also report, there are other factors such as surface contamination, surface vibration, filaments not at initial rest, temperature driven effects, as well as generated filaments not being completely symmetrical, that can lead to possible differences between the results.)

We explore the above non-continuous behavior in more details; as shown in fig. 9, a subtle competition between inertial effects, oscillating modes, and capillarity, can lead to this peculiar dynamics: for sufficiently small Oh numbers, the time scale over which the filament retracts is comparable to the time scale over which the surface instabilities grow. Meanwhile, due to inertial effects, capillary waves propagate on the surface, which are dampened by the viscous effects. From looking at fig. 9(b), it is clear that the capillary waves develop on the surface; if the oscillation of the capillary waves happens at the time of the breakup, it can eventually prevent the necking of the filament and the consequent breakup. For a small Oh number, internal flows are important, unlike for highly viscous filaments. Additionally, the time scale of collapse is comparable with the typical time scale on which capillary waves propagate. The transition from no-breakup to breakup can therefore become sensitive to when all these effects are in balance, showing a non-continuous behavior. Future work should

consider quantifying each effect to provide a more in depth analysis of the transition mechanism.

In summary, our study of free-standing filaments reveal a remarkable agreement with the experimental results obtained in [7]. We also observe that a liquid filament with Oh number greater than 1 never breaks up regardless of the filament aspect ratio. Additionally, we extend the range of parameter space to very small Oh numbers where there is a rich spectrum of dynamics present. We show how subtle interplay of the dynamical effects can lead to unexpected outcomes. We next focus on the transition from no-breakup to breakup including substrate effects. We also study the influence of slip on the breakup transition and discuss the specific regions where a remarkably different behavior occurs when compared with the free-standing jets.

3.1 Transition from no-breakup to breakup including substrate effects

Here we consider finite-size filaments deposited on a substrate that retract axially and either break up during the retraction or collapse into a single droplet. As discussed earlier, for viscous filaments, we also observe in this case that as the tails of the filament recede, two bulges form at the end of the filament. As the bulges grow, a neck that connects the bulges to the filament forms. Figure 10 shows a typical simulation image of the necking process just prior to the breakup. From inspecting the velocity field, we see how the fluid is squeezed out from the neck to the bulge, while the filament is retracting. If the time that the bulges have to travel before collapsing in the middle is smaller than the time required for the neck to pinch off, then the filament will not break up during the traction process, creating a strong vortical flow at the neck. The color map also shows an area of high pressure at the ridge connecting the bulge to the filament in the middle. Our aim is to investigate this process and the dynamics resulting the breakup. We extend the results discussed above for a free-standing filament to include the substrate effects. The introduction of the substrate is expected to profoundly change the dynamics by delaying the retraction of the tails of the filament and therefore allowing for the instabilities to have sufficient time to grow, promoting breakup. For small to moderate Oh values, where the breakup occurs due to either the end-pinch-off or the Rayleigh-Plateau instability developing on the filaments connecting the end bulges, the inclusion of the substrate results in smaller critical aspect ratio than the one for the free-standing filament. A striking conclusion of our study is that for very viscous filaments, *i.e.* for $Oh > 1$, the filament still breaks up due to the Rayleigh-Plateau instability, in contrast to the results of simulations and observations described in the previous section for free-standing filaments. One experimental example of this effect was shown in fig. 3.

As noted above, the breakup of the filament on the substrate can be largely influenced by the retraction velocity of the tails of the filament. Providing a theoretical explanation of the critical AR that leads to breakup is however

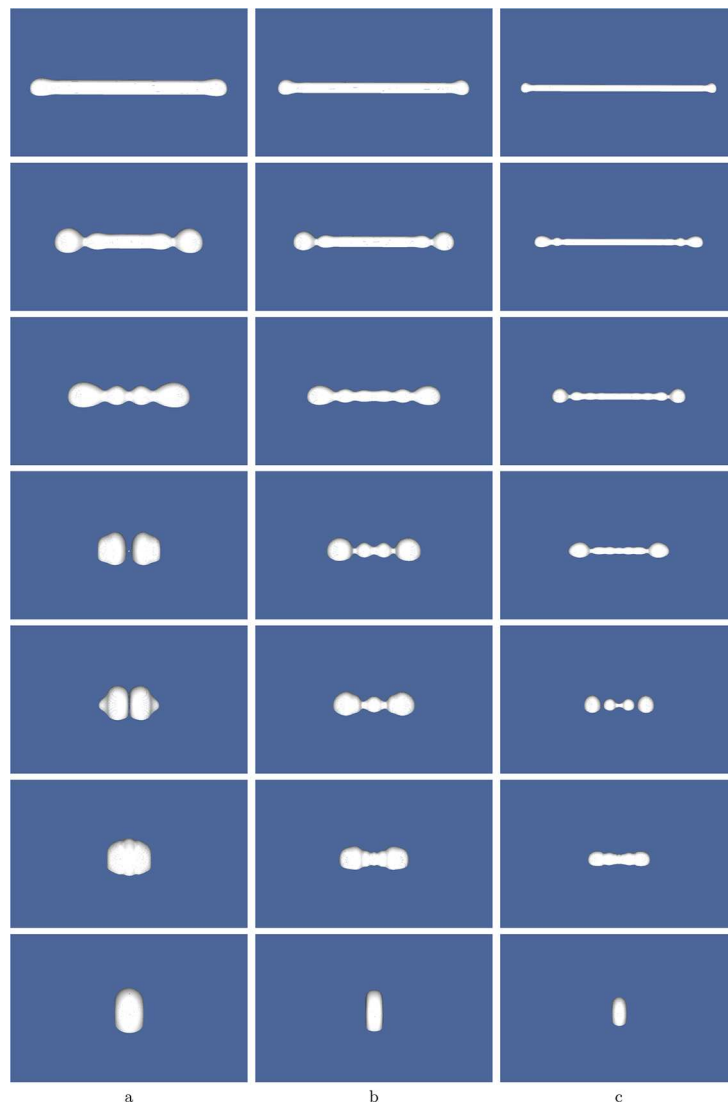


Fig. 9. Simulations for free-standing jets for $Oh = 0.02$, (a) $AR = 12$, (b) $AR = 16$ and (c) $AR = 26$. Only the top half of the filament is shown.

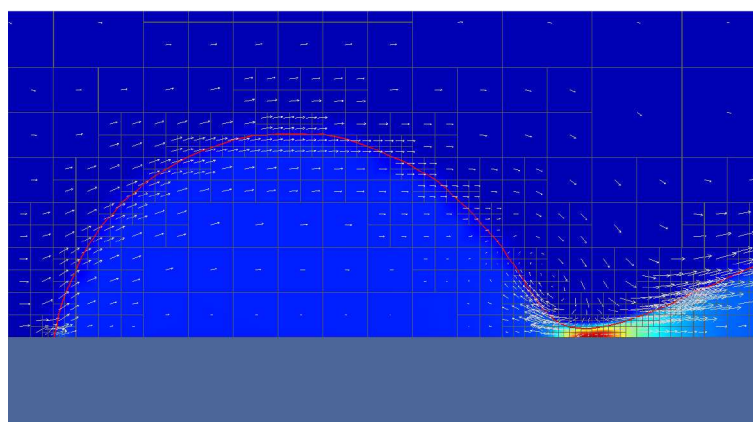


Fig. 10. Zoom of a cross section ($z = 0$) of the bulge and the neck region prior to breakup, showing the details of the flow field (white arrows) and the pressure distribution (red (blue) shows the areas of high (low) pressure); the background shows the adaptive mesh. $Oh = 0.2$, $AR = 33$, and $\lambda = 0$.

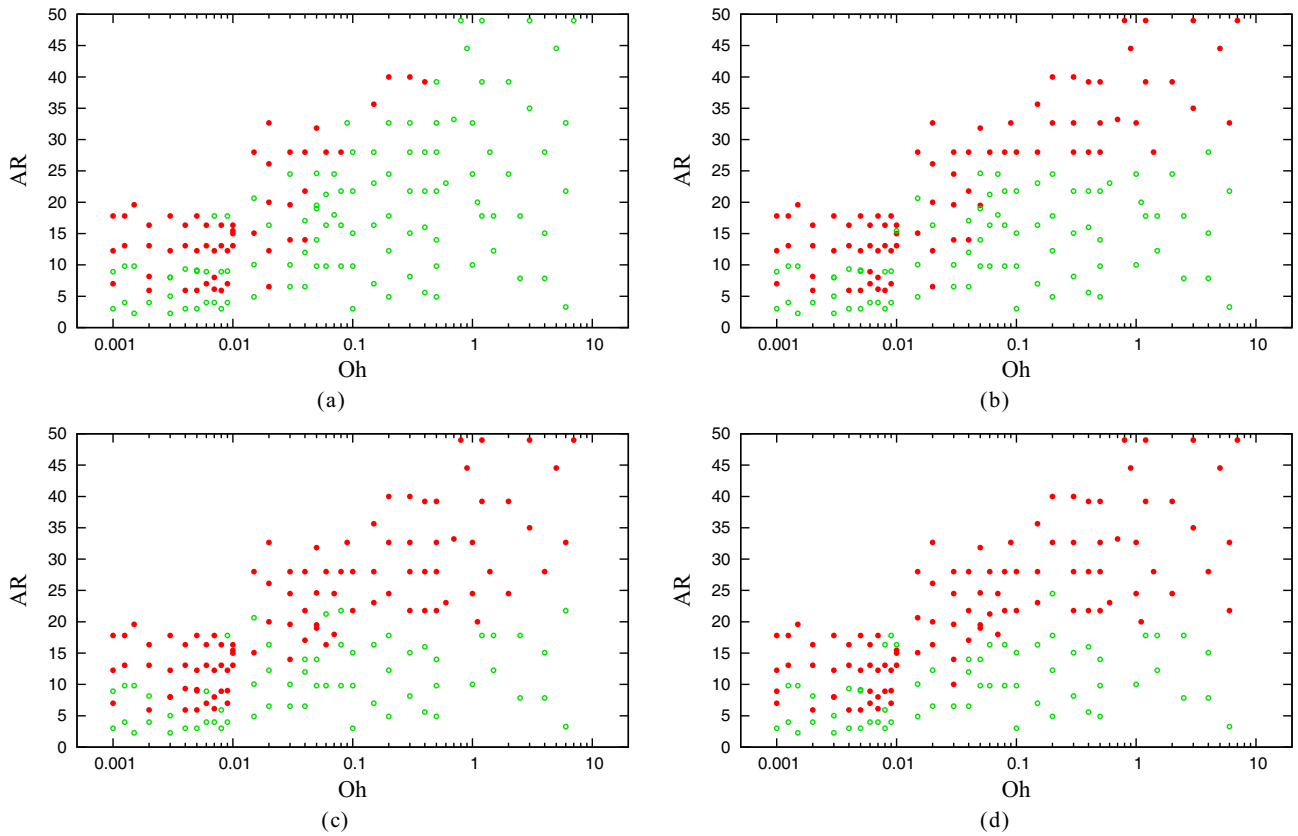


Fig. 11. Breakup and no-breakup results plotted as a function of Oh *versus* AR: breakup (●) and no-breakup (○), for $\lambda = 1$ (a), 0.1 (b), 0.01 (c), and 0 (d).

difficult due to the fact that the typical velocity of tails of the filament cannot be found analytically, mainly as a result of the contact line singularity and issues related to that; see *e.g.* [17]. It is the aim of the following study to provide a numerical database to characterize the no-break to breakup regions based on the extent of the slip on the substrate. We consider various levels of slip, defined by λ in eq. (1), and repeat the numerical simulations for a range of Oh and AR values. We note that the case of a perfect slip condition at the substrate corresponds to the free-standing filaments. In our numerical model, we impose a Navier slip through eq. (1); when $\lambda = 0$, this condition amounts to a no-slip condition on the velocity field. Here, we consider $\lambda = 0, 0.01, 0.1, 1$ and carry out an exhaustive study of the effect of slip on the breakup transition.

Figures 11(a)–(d) show how the breakup transition depends on the slip length: in general, the critical AR of the breakup decreases with a decrease of λ . This can be understood based on the fact that the retraction of the filament ends is decelerated by decreasing the amount of slip (*i.e.*, by increasing the viscous dissipation at the contact line), which leaves sufficient time for the necking and/or the Rayleigh-Plateau instability to occur. Clearly, as the slip length is decreased, the transition from no-breakup to breakup is shifted down, including more data points that represent a breakup. For small Oh (< 0.01) however there are anomalies where the breakup transitions to

no-breakup (and again to breakup) when increasing the amount of slip; this is mainly due to a complex and subtle interaction with inertial effects. Next, we elaborate on these competing effects.

To provide more insight into the effect of slip on the breakup transition, we show in fig. 12(a)–(d), a sequence of simulations for a moderate Oh = 0.15 and relatively large AR = 28, for $\lambda = 1, 0.1, 0.01, 0$. As seen, the transition from no-breakup to breakup on a substrate depends on subtleties in the problem arising from certain situations at the moment of the breakup: (a) breakup may not occur for a large slip $\lambda = 1$ as the retraction speed is fast so the thinning of the neck happens as the end bulges get too close to each other preventing further necking and the pinch-off; (b) for a moderate slip, $\lambda = 0.1$, breakup occurs due to end-pinching which happens at the middle of the filament—the resulting droplets however merge due to inertial effects; (c) for a small slip, $\lambda = 0.01$, both necking at end points and the Rayleigh-Plateau instability in the middle are operative at the same time—however, the instability in the middle wins over the end-pinching leading to the formation of two stable droplets; and (d) for zero slip, $\lambda = 0$, the filament breaks up due to both mechanisms—end-pinching and the instabilities growing in the middle due to the development of capillary waves, resulting four primary droplets in this case.

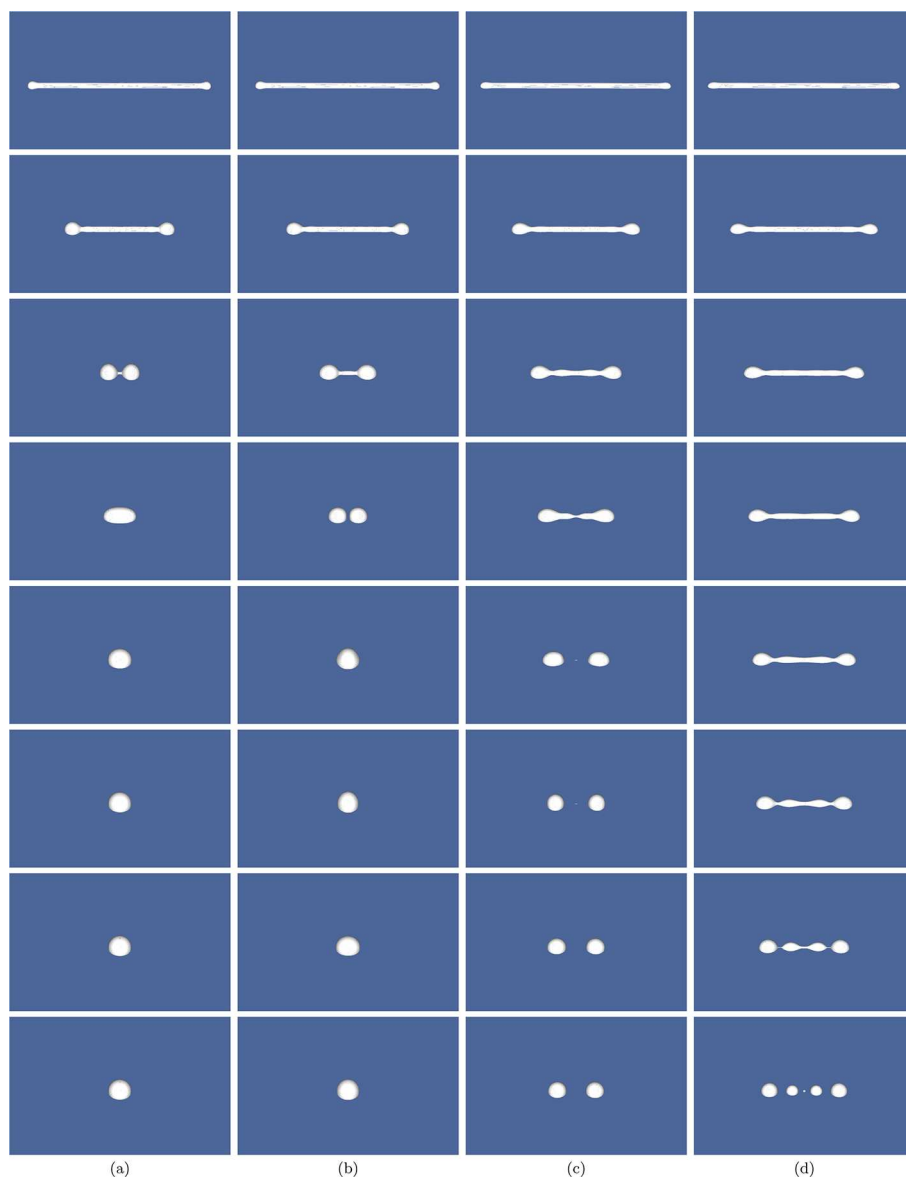


Fig. 12. Snapshots of the simulations revealing various scenarios for $Oh = 0.15$ and $AR = 28$, and for $\lambda = 1$ (a), 0.1 (b), 0.01 (c), and 0 (d).

4 Conclusions

This work presents an extensive computational study of the breakup of finite-size liquid filaments, including substrate effect, using direct numerical simulations. We carry out detailed computations to provide an enhanced understanding of the subtle and complex competition between the end-pinching and the Rayleigh-Plateau instability that leads to the transition from no-breakup to breakup region in the parameter space that we consider. We focus on the effects of Ohnesorge number, the filament aspect ratio, and slip length; we did not consider the effect of the contact angle due to the limitation existed in the numerical framework and leave the study of this effect to future work. We however note that a prior work in the literature

has considered such effect [10] and the interested reader is referred to this study for further discussions. Additionally, we refer to the work carried out by two of the co-authors on the issues related to the computations of moving contact line problem [17]. Nevertheless, our study provides a most complete picture, that has not been available in the literature so far, of the breakup of finite-size filaments, when also considering the substrate effect.

Our study also provides detail insight into various scenarios, namely, a collapse into a single droplet, the breakup into one or multiple droplets, and recoalescence into a single droplet after the breakup (or even possibly another breakup after recoalescence), and finally the formation of distinct droplets when there is the substrate effect. We also show that when there is a slip effect, the

liquid filament can break up for large Oh (> 1), considerably different from free-standing filaments that show no breakup for this case regardless of the AR value. Our comprehensive results significantly extend the available parameter space over which the transition from no-breakup to break occurs, when also including the substrate effect. We observe how the retraction velocity of the end points on the substrate can strongly influence this transition. A careful comparison of the retraction speed with experimental results will allow the calibration of the slip length, whose understanding clearly requires future work.

This research was partially supported by the NSF grant No. CBET-1604351. We gratefully acknowledge Kim Lozarito, Michel Castor, Matthew Marner, Elise Burkhardt, and Brandon DeGraw for carrying out the experiments. SA gratefully acknowledges helpful discussions with S. Zaleski.

Author contribution statement

A. Dziedzic, M. Nakrani, B. Ezra, and M. Syed carried out all the simulations, performed the analysis, and generated the visualizations. S. Popinet created the simulations example and authored the numerical code. S. Afkhami conceived the project, planned the simulations, and wrote the first draft of the manuscript. All authors discussed, edited, and revised the manuscript.

Publisher's Note The EPJ Publishers remain neutral with regard to jurisdictional claims in published maps and institutional affiliations.

References

1. J.R. Lister, H.A. Stone, *Phys. Fluids* **11**, 2758 (1998).
2. J. Eggers, *Phys. Rev. Lett.* **71**, 3458 (1993).
3. J. Eggers, *Rev. Mod. Phys.* **69**, 865 (1997).
4. O.A. Basaran, *AIChE J.* **49**, 1842 (2002).
5. P.K. Notz, O.A. Basaran, *J. Fluid Mech.* **512**, 223 (2004).
6. J.R. Castrejón-Pita, N.F. Morrison, O.G. Harlen, G.D. Martin, I.M. Hutchings, *Phys. Rev. E* **83**, 036306 (2011).
7. A.A. Castrejón-Pita, J.R. Castrejón-Pita, I.M. Hutchings, *Phys. Rev. Lett.* **108**, 074506 (2012).
8. T. Driessen, R. Jeurissen, H. Wijshoff, F. Toschi, D. Lohse, *Phys. Fluids* **25**, 062109 (2013).
9. C.A. Hartnett, K. Mahady, J.D. Fowlkes, S. Afkhami, L. Kondic, P.D. Rack, *Langmuir* **31**, 13609 (2015).
10. G. Ghigliotti, C. Zhou, J.J. Feng, *Phys. Fluids* **25**, 072102 (2013).
11. I. Cuellar, P.D. Ravazzoli, J.A. Diez, A.G. González, *Phys. Fluids* **29**, 102103 (2017).
12. S. Popinet, *The Gerris flow solver* (2012) 1.3.2, <http://gfs.sourceforge.net/>
13. J. Diez, A.G. González, J. Gomba, R. Gratton, L. Kondic, *Physica D* **209**, 49 (2005).
14. L. Rayleigh, *Proc. London Math. Soc.* **1**, 4 (1878).
15. S. Popinet, *Savart-Plateau-Rayleigh instability of a water column*, <http://gfs.sourceforge.net/examples/examples/plateau.html>.
16. S. Afkhami, S. Zaleski, M. Bussmann, *J. Comput. Phys.* **228**, 5370 (2009).
17. S. Afkhami, J. Buongiorno, A. Guion, S. Popinet, Y. Saade, R. Scardovelli, S. Zaleski, *J. Comput. Phys.* **374**, 1061 (2018).
18. S. Popinet, *J. Comput. Phys.* **190**, 572 (2003).
19. S. Popinet, *J. Comput. Phys.* **228**, 5838 (2009).
20. S. Popinet, *Annu. Rev. Fluid Mech.* **50**, 49 (2018).
21. K. Mahady, S. Afkhami, L. Kondic, *Phys. Fluids* **27**, 092104 (2015).